RSC Advances

ROYAL SOCIETY OF CHEMISTRY

www.rsc.org/advances

RSC Advances

RSCPublishing

ARTICLE

Phytosynthesis of Silver-Reduced Graphene Oxide (Ag-RGO) nanocomposite with enhanced antibacterial effect using *Potamogeton Pectinatus* extract.

Cite this: DOI: 10.1039/x0xx00000x

Received 00th January 2012,
Accepted 00th January 2012

DOI: 10.1039/x0xx00000x

www.rsc.org/

Mohammed S. Abu El-Hassan,† Mona B. Mohamed,‖ Manal Fawzy,§ Dalia A. Abdelrehim,‡ and Mohamed M.S.A. Abdel-Mottaleb *,†

ABSTRACT: A new green synthesis method for preparation of silver-Reduced Graphene Oxide (Ag-RGO) nanocomposite using *Potamogeton Pectinatus (Po)* plant extract is introduced. Size, morphology and crystallinity of the as-prepared nanomaterials were studied with an explanation for the role of *Po* in synthesis. A preliminary antibacterial experiment was developed to ensure the enhanced antibacterial effect of Ag-RGO nanocomposite. The antibacterial measurements were done using Colony Counting method. Results indicated that the majority of Silver Nanoparticles "AgNPs" were formed in a spherical shape with small sizes ranging from 11 to 20 nm. IR spectroscopy results indicated the role of amine and hydroxyl groups from *Po* in the reduction and capping processes. The preliminary antibacterial examination ensured the enhanced antibacterial effect of Ag-RGO nanocomposite.

Introduction:

Metal nanoparticles and their nanocomposites, especially silver nanoparticles (AgNPs), attracted attention of scientists worldwide in the recent years due to their unique physical and chemical properties. These unique properties, which are attributed to their small sizes and large surface area, made them highly applicable in different areas such as catalysis, electrical conductivity, DNA sequencing, antimicrobial and antibacterial activities, Surface Enhanced Raman spectroscopy (SERS), and drug delivery systems.[1-6] Different approaches were applied for AgNPs production, such as chemical reduction and photo-reduction in reverse micelles,[7] thermal decomposition in organic solvents,[8] and radiation chemical reduction,[9-11] but most of them are either expensive or produces toxic and hazardous by products which affect the environmental ecological systems.[12] Hence, there is a strong need for green synthesis methods with no remarkable toxic chemicals especially for application in the biomedical field.[13]

Po is a widely distributed submerged macrophyte.[14-16] Its abundance is very high in Egypt, Africa, Asia, North and South America. The latest publications about *Po* showed that it is rich in polyphenolic compounds, proteins, amino acids and carbohydrates,[17-19] which act as reducing and stabilizing agents for nanomaterials preparation. Polyphenolic compounds, especially, Flavonoids chelate metal ions and then reduce them through donation of electrons or hydrogen atoms.[20-25] Role of protein, found in Po, can by summarized as a reducing agent by amine and caroxylate groups [23,26-29] and a capping and stabilizing agent by carbonyl groups which bind to metal nanparticles and stabilize them.[23,30,31]

According to the above discussed advantages and abundance, *Po* is an excellent candidate for green, safe and economic fabrication of nanometrials and hence, we use this plant for the first time in preparation of Ag-RGO nanocomposite in this thesis work.

The effectiveness of antibiotics for treatment of infectious diseases caused by pathogenic bacteria is lowered by the rise of microbial drug resistance, resulting in poor treatment efficacy of these drugs and significant economic losses.[32-36] Nanotechnology introduced many nanomaterials as antibacterial agents during the last decade. The most promising example of such nanomaterials is Silver nanparticles (AgNPs).[37-39] AgNPs are used in many applications to inhibit bacterial growth, such as in dental work, catheters and burn wounds.[40,41] The mechanism behind antibacterial effect of AgNPs is still not completely clear but many theories introduced acceptable interpretations. AgNPs introduce morphological and structural changes in bacterial cells. The general understanding is that AgNPs bind to sulfur-containing proteins of cell membrane and physically make “pits” in it with changing membrane permeability, resulting in cell death.[42, 43] Furthermore, AgNPs make drastic changes inside bacterial cells as they bind to phosphorous moieties in DNA and prevent its replication, or react with sulfur-containing proteins of enzymes and inhibit their functions; hence the inhibition of cells division.[44, 45] As well, many papers discussed reactive oxygen species (ROS) and free radicals affiliated effects.[46]

Graphene oxide (GO) nanosheets are well known for their strong antibacterial effect.[47] The antibacterial effect of GO nanosheets is explained via two combined mechanisms; the first one is the direct physical stress of sharp edges of these nanosheets on cell wall, resulting in its fracture, while the oxidative stress action on cell membrane is the second mechanism.[48, 49]

The combination of AgNPs with GO nanosheets in a composite of Ag-RGO resulted in a synergetic antibacterial action, as both components work on cell membrane damage and oxidation of the main components of bacterial cells, resulting in cell death.[50, 51] As a potential antibacterial material, this composite must be synthesized using green methods.

Here, we introduce the synthesis of Ag-RGO using *Po* extract in a continuation for a method we previously reported (AbdelHamid et al).[17]AbdelHamid synthesized AgNPs, AuNPs and Ag-Au alloy using this plant extract. In this paper, we elaborate on the action mechanism of plant extract and further investigate the effect of temperature. Additionally, we investigate the antibacterial effect of Ag-RGO in a comparison with that of GO nano sheets.

Materials and Methods:

Materials. Graphite powder (≥ 99.99 %) was purchased from SIGMA-ALDRICH and used as received for synthesis of graphene oxide nanosheets. Potassium Permanganate (KMnO4, 99%), Phosphoric acid, 30% H_2O_2, 98% H_2SO_4, 37% HCl, were purchased from SIGMA-ALDRICH. Silver Nitrate salt was purchased from Sigma Aldrich, USA and used as received.
Po was collected by prof. Manal Fawzy (Environmental science department, faculty of science, Alexandria University) from Lake Marriott which is one of the Nile Delta Lakes in Southern Alexandria, Egyptian spring, 2013. Samples were immediately transferred to the lab, washed thoroughly with de-ionized water twice, then dried in an oven at 60^{o}C until reaching a constant weight of the dried plant and then grinded in a stainless steel mortar.

E. coli 107 bacteria were acquired from Botany department, faculty of science, Sohag University, Egypt. The components of growth medium, Luria-Bertani (LB), were supplied from Difco laboratories.

Synthesis of Graphene Oxide (GO) nanosheets. GO nanosheets were prepared from graphite powder using Improved Hummer's Method (IHM).[52] In this method, 1 g graphite powder is added to a mixture of 120 ml concentrated Sulfuric acid and 13 ml Phosphoric acid in an ice bath at 15^{0}C. The mixture is stirred till homogeneity, 30 minutes. After that, 6 grams of Permanganates were added to the reaction mixture portion wise for an hour. Then, the temperature was elevated to 45^{0}C while stirring for 3 hours. Then, 150 ml distilled water mixed with 20 ml Hydrogen peroxide 30% were added to stop the reaction. The GO nanosheets are then filtered off using centrifugation and washed with HCl and distilled water until the complete removal of sulfates, chlorides and other contaminants. Finally, the obtained GO nanosheets are dried overnight in an oven at less than 65^{0}C.

Preparation of Potamogeton pectinatus plant aqueous extract. The plant was powdered well and then 1.5 gm of the powder was added into a conical flask containing 25ml distilled water. The mixture was gently heated at 70^{o}C for 30 minutes under magnetic stirring. The solution was then filtered through Whatman filter paper No-1. The solution was kept in refrigerator at 4^{o}C for further synthesis of nanomaterials.

Synthesis of Silver-Reduced Graphene Oxide (Ag-RGO) nanocomposite. Synthesis of this nanocomposite was completed in two main steps; the first was to prepare GO-Ag suspension with no excess of Ag^{+} ions, in order to ensure an accurate measurement for the formation of Ag-RGO nanocomposite and not AgNPs separate from GO nanosheets. The second step was to reduce GO-Ag into Ag-RGO nanocomposite by using plant extract as a reducing and capping agent.

Preparation of GO-Ag suspension. 1ml of GO suspension (its concentration: 5 mg/L) was added to 50 ml solution of 10^{-1} M $AgNO_3$ and were stirred for 2hrs. A centrifugation step was done to eliminate the excess of Ag^{+} ions. The precipitate, Ag-GO, was washed by distilled water and re-suspended in 15ml distilled water.

Reduction of GO-Ag suspension into Ag-RGO nanocomposite via Po plant extract. 4 ml of extract were added to the suspension of GO-Ag, the solution was stirred for 4 hours (hrs) at 70^{o}C and the UV/Vis spechtrophotometric measurements and TEM images were carried out each hour. The experiment was repeated at 90^{o}C and the absorbance was measured after 3 hrs of stirring. The excess plant extract can be removed by centrifugation at 7000 rpm for 10 minutes. Furthermore, FTIR analysis was carried out for plant extract at 70^{o}C and at 90^{o}C to investigate changes in extract structure. Additionally, some of Ag-RGO nanosheets were precipitated, dried and characterized via XRD analysis.

Antibacterial action of GO and Ag-RGO nanocomposite. The antibacterial action of GO and Ag-RGO nanomaterials was studied on E. coli 107 bacteria by The colony counting method.

Cell preparation. E. coli 107 cultures were grown in Luria-Bertani (LB) broth, aerobically, at 37^{o}C in incubator. The broth contained Peptone 5g, Yeast 3g and NaCl 5g. The cells were harvested by centrifugation at 5000 rpm for 15 minutes. Then, washed for three times by phosphate-buffer saline solution (PBS) and re-suspended in the nutrient medium. The initial concentration of bacteria was diluted many times until reaching the colony count of 10^{6} – 10^{7} CFU/ml.

Comparison between the antibacterial effects of GO and Ag-RGO nanosheets. A 5 ml saline solution of GO or Ag-RGO (100 µg/ml) was incubated with a 5 ml saline solution of E. coli 107 bacteria (10^{6}-10^{7} colony forming units per milliliter (CFU/ml) for 4 hrs at a 250 rpm shaking speed and 37^{o}C. In parallel, isotonic saline solution of E. coli without treatment was used as a control. Loss of cell viability of E. coli was measured using colony counting method, in which a series of 10-fold cell

dilutions (120 µl for each one) were spread onto LB plates and left overnight to grow at 37°C. After that, colonies count of these plates was compared to that of control. All treatments were done at least twice.

Characterization:

UV/Vis spectrophotometer (SHIMADZU, Japan, model UV21650 PC) was used to monitor synthesis of nanomaterials and detect their absorption bands. Raman spectroscopy (WITec instruments Corp, Germany) was applied on GO samples to detect the D and G characteristic bands of GO nanosheets. FTIR spectroscopy (Nicolet 6700) was applied on IHM GO to detect the main functional groups. It was applied also on *Po* extract before and after synthesis of Ag-RGO nanocmposite at low temperature and at a high temperature to detect the functional groups of the extract and to understand the chemical changes of its structure under different conditions. TEM analysis (JEOL TEM-2100) at 200 KV was carried out for RGO-Ag nanocomposite under different conditions. XRD analysis (Shimadzu, Kyoto, Japan) with a scanning angle ranges from 8 to 28 2Theta for IHM GO nanosheets and from 10 to 80 2Theta degrees were carried out for RGO-Ag powder samples.

Results and Discussion:

Synthesis and characterization of GO nanosheets. The brown GO nanosheets were prepared from the black graphite powder by means of strong oxidation, figure (1A), using Improved Hummer Method (IHM).[52] This method depends on addition of excess Sulfuric acid mixed with Phosphoric acid and a higher amount of Permanganate to provide strong oxidation conditions. The oxidation of graphite (Gt) produced graphite oxide (GtO) with many oxygen-containing groups.

The FTIR analysis confirmed the formation of many oxygen-containing groups,[53] such as hydroxyl (OH) (stretching at 3434 cm^{-1}), C-H (stretching at 2849.81 cm^{-1}) and 2921.74 cm^{-1}, carbonyl (C=O) at 1720 cm^{-1}, unsaturated double bonds (C=C) at 1627.64 cm^{-1}, and COOH at 1726.10 cm^{-1} for the C=O part and the significant broadening from 3434 to 2500 cm^{-1} due to hydrogen bonding of OH groups, figure (1B). The introduction of these oxygen-containing groups resulted in the increase of the interlayer spacing between graphite sheets but did not exfoliate them totally. Sonication processes resulted in exfoliation of GtO sheets into GO nanosheets which contain a small number of stacked layers. These stacked nanosheets have a longer interlayer distance which was characterized by XRD analysis, figure (1C).

In the XRD analysis, the 2Theta value was shifted from 26°, which is the normal value for graphite powder,[54] into 2Theta = 9.5°, which reflects an interlayer spacing (d of GO nanosheets with a value 9.2 A°. The complete disappearance of the value 26° for 2Theta means a complete oxidation process. This is illustrated in figure (1c).

The Raman spectra of Improved Hummer method synthesized GO "IHM GO" in figure (1D), showed presence of the intense D-band at 1350 cm^{-1} (the band referring to lattice distortion) and the normal G-band at 1590 cm^{-1}. The D-band is attributed to the high level of oxidation which resulted in defects on GO nanosheets surface and lattice distortion.[55]

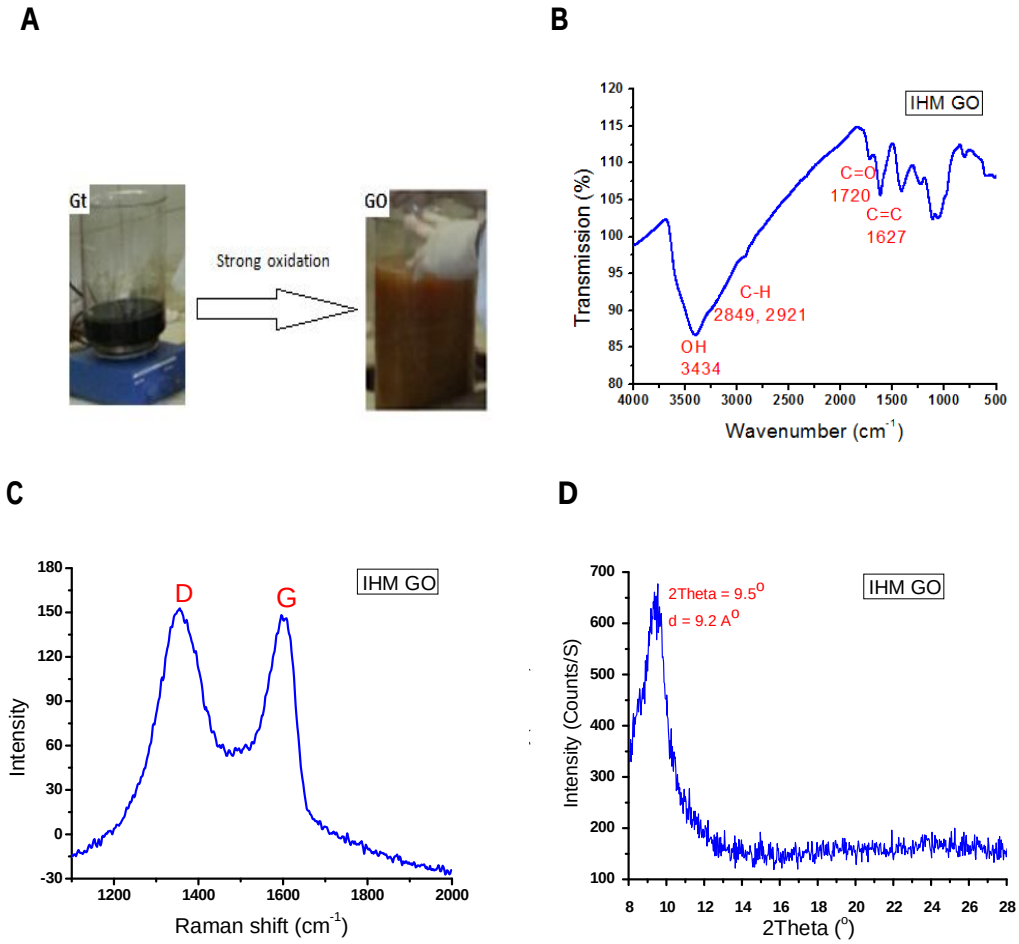

Figure 1. Gt oxidation using IHM to be converted into GO nanosheets (A). FTIR analysis of the as prepared GO nanosheets which demonstrates the different functional groups on surface and edges (B). The XRD analysis of GO nanosheets demonstrating a complete oxidation with no bands for residuals of Gt (C). Raman analysis indicating D and G-bands of GO nanosheets (D).

Synthesis of Ag-RGO nanocomposite. Figure (2A) illustrates a schematic diagram for synthesis of Ag-RGO nanosheets from graphite powder. The procedure depends on two steps; the first is the chemical and physical binding of Ag^+ ions onto GO nanosheets and the second is the reduction of both Ag^+ and GO where AgNPs become part of RGO nanosheets. GO nanosheets were immersed in $AgNO_3$ solution and stirred for two hours where active sites of GO are saturated by Ag^+ ions and then separated from excess silver nitrate solution by centrifugation. The separated GO-Ag complexes were re-suspended in 15 ml distilled water and were reduced by the plant extract. The challenge is monitoring Ag^+ reduction on surface of GO nanosheets. Despite having strong surface plasmon resonance (SPR) which depends on their shape and size,[56-58] AgNPs had no detectable SPR peaks while being in the form Ag-RGO. This is attributed to the quenching effect of GO nanosheets for SPR of metal nanoparticles.[59,60] One possibility is to measure absorption peaks of AgNPs. Yet this is not accurate; excess Ag^+ is needed to have a detectable signal which results in the observation of free AgNPs peaks and not Ag-RGO ones.[61-63]

As discussed above, UV-Visible (fig 2B) is not possible for investigation of the Ag-RGO nanocomposite. On the other hand, TEM is an excellent tool to monitor the synthesis process by taking TEM images at specific time intervals during the synthesis process.

The TEM images of the as-prepared samples are illustrated in figure (2C-F). Figure (2C) is a TEM image of GO nanosheets that indicates the layer-like nature of GO nanosheets. Figure (2D) is a TEM image of the mixture of GO-Ag and *Po* extract after 2 hours of reduction, which indicates formation a few numbers of AgNPs on surface of RGO nanosheets. As the reduction process continued, more AgNPs were precipitated on surface of RGO. This was clear in the TEM image of Ag-RGO nanocomposite after 4 hours of reduction, figure (2E). On the other hand, AgNPs were well distributed on surface of RGO nanosheets with a majority of spherically-shaped nanoparticles, figure (2E, inset). In addition, particle size distribution in figure (2E, inset) of AgNPs on surface of RGO nanosheets demonstrated that 66% had diameters between 11 and 20 nm, 24% were ranging from 21 to 30 nm, 5% were ranging from 1 to 10 nm and the last 5% were between 31 to 40 nm in diameters. From HR-TEM image of Ag-RGO nanocomposite in figure (2F), nature of binding between AgNPs and RGO nanosheets appeared similar to metal-metal fusion with some surface defects in AgNP due to stacking to edges of RGO nanosheets. The polycrystalline nature of AgNPs was demonstrated by the Selected Area Electron diffraction (SAED) pattern of AgNPs on surface of RGO nanosheets with concentric rings of crystal planes, figure (2F, inset). These crystal planes were interpreted as (111), (200), (220) and (311) of face centered cubic (FCC) lattice by XRD analysis of Ag-RGO. There is a plane with indices of (111) was written in red on the SAED pattern to indicate presence of AgCl crystals as impurities.

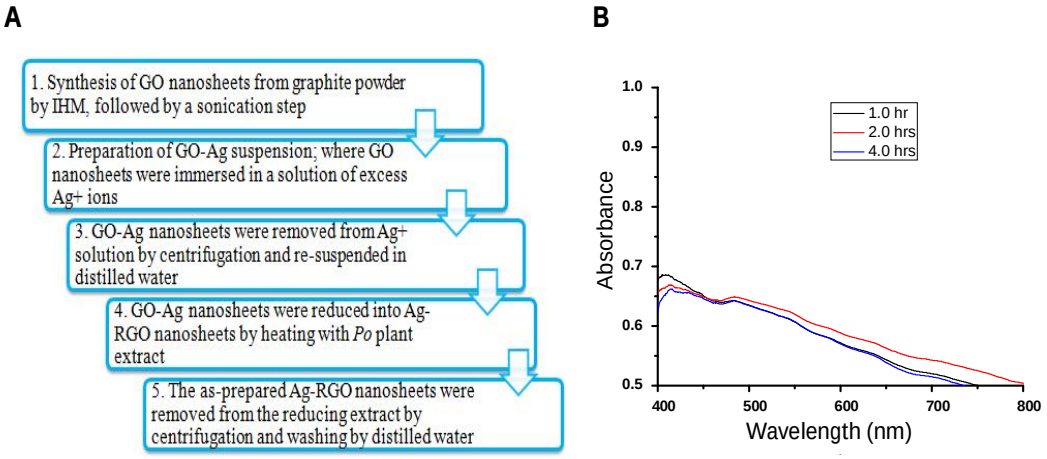

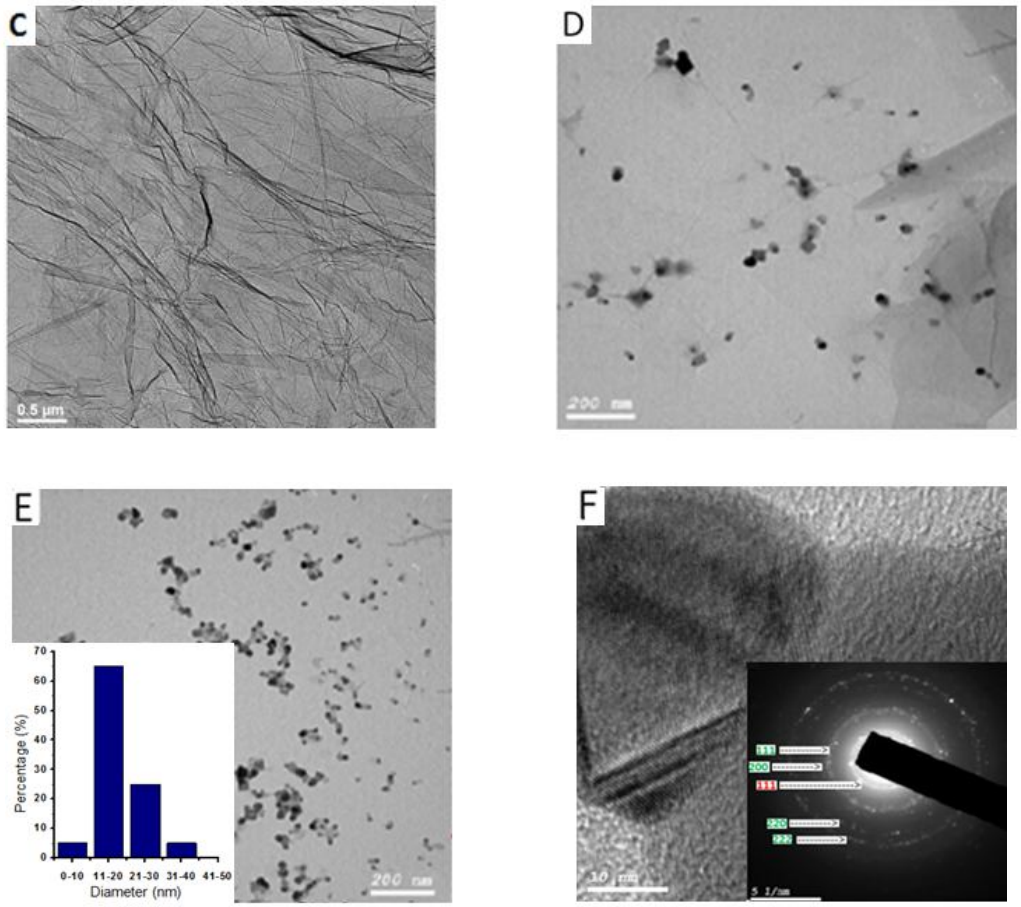

Figure 2. A schematic diagram for synthesis of Ag-RGO nanosheets (A), UV-Vis spectral analysis of Ag-RGO nanocomposite without detectable results for AgNPs plasmonic peaks on surface of RGO nanosheets (B), TEM image of GO nanosheets, (C), TEM image for a mixture of GO-Ag and Po extract after 2 hours of reduction where some AgNPs were formed on surface of RGO nanosheets (D), more AgNPs were precipitated on surface of RGO after 4 hrs of reaction (E), particle size distribution of AgNPs on surface of RGO nanosheets (E, inset), HR-TEM image of Ag-RGO nanocomposite indicating nature of binding between AgNPs and RGO nanosheets which appeared similar to metal-metal fusion with some surface defects in AgNPs due to stacking to edges of RGO nanosheets (F), the crystalline nature of AgNPs are also illustrated by the Selected Area electron diffraction (SAED)-TEM image (F, inset)

The XRD analysis of IHM GO nanosheets and IHM RGO-Ag nanocomposite in figures (3A & 3B) indicated many important observations. GO showed a strong diffraction peak at 2Theta = 9.5 degrees with an interlayer distance of 9.2 A^o (figure 3A). After reduction process, GO peak was shifted into 2Theta = 12.27 degrees with an interlayer distance of 7.2 A^o due to partial reduction of some oxygen-containing groups on surface of GO nanosheets. On the other hand, a new peak appeared at 2theta = 23 degrees for RGO nanosheets formation, figure (3B). Hence, the product contains both the fully reduced GO and the partially reduced GO nanosheets. Second, the Ag nanoparticles' introduced weak diffraction peaks at 38.24^o, 44.54^o, 64,65^o and 77.12^o which correspond to (111), (200), (220) and (311) planes of FCC lattice of AgNPs, respectively (JCPDS card No: 04-0783), figure (3B). Third, the diffraction peaks of planes (220) and (311) appeared at 64,65^o and 77.12^o which are slightly different

from the standard values of 64.44 and 77.42° (JCPDS card No: 04-0783). This very small difference is attributed to surface defects in lattice of the produced AgNPs due to their stacking to RGO nanosheets. Fourth, AgCl crystals were formed during reduction process with slightly strong diffraction peaks as illustrated in figure (3B) (JCPDS card No: 31-1238). These AgCl crystals were precipitated from the combination of Ag^+ ions from $AgNO_3$ solution with Cl^- ions from the extract. Finally, the unassigned two diffraction peaks in figure (3B) might be attributed to the bio-organic crystals of plant extract.

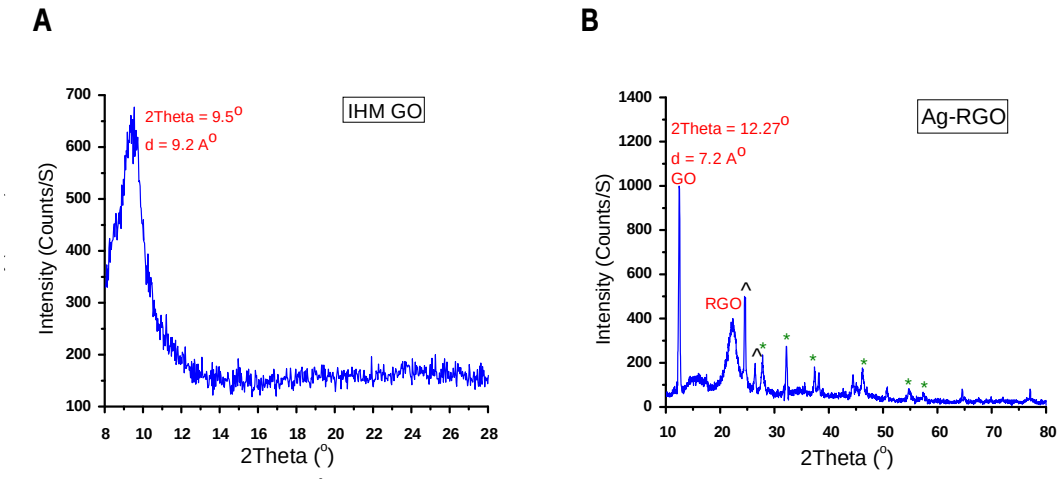

Figure 3. The XRD analyses of IHM GO nanosheets (A), and IHM RGO-Ag nanocomposite (B). Diffraction peaks of AgCl as impurities (*), Crystallographic planes [(111), (200), (220), 311)] of AgNPs on surface of RGO nanosheets, and the unassigned diffraction peaks which might be attributed to the bio-organic crystals of plant extract organic components (^).

RSC Advances RSCPublishing

ARTICLE

Role of *Po* plant extract in formation of Ag-RGO nanocomposite. Potamogeton pictinatus plant extract contains polyphenolic compounds, proteins with free amino acids and carbohydrates[17-19] with electron donating groups. These compounds act as reducing and capping agents. Their capping property is attributed to presence of long-chain compounds of proteins and carbohydrates.[17] The FTIR analysis of Po plant extract, figure (4A), show presence of amine groups stretching vibrations with two adjacent peaks at 3370 and 3462 cm^{-1}, hydroxyl groups stretching at 3410 cm^{-1}, Nitrile (CΞN) groups stretching vibrations at 2333 cm^{-1}, C=C groups stretching vibrations at 1645 cm^{-1} and N-H Wagging (bending) vibration modes at 676.9 cm^{-1}. Temperature variation has a strong effect on catalytic degradation of Potamogeton pictinatus extract by GO nanosheets during reduction process. *Po* extract works as a reducing and capping agent in synthesis of AgNPs as demonstrated in our previous paper[17] and for GO nanosheets, too. The difference between this reduction and reduction of Ag^+ ions is that GO undergoes catalytic degradation of the extract, especially at elevated temperatures. At 70°C, the FTIR absorption peaks of amine and hydroxyl groups in figure (4B) decrease in intensity, if compared to those of extract while the other peaks of C=C or CΞC increase in intensity. That indicates that, beside the reduction of Ag^+ ions into AgNPs, the extract itself was slightly degraded and changed in structure. On the other hand, this change was drastic when temperature increased to 90°C and the decomposition of the extract was more significant. There were no detectable peaks for amine groups and there was only a broad band at 3410 cm^{-1}, figure (4C). This is also clear from the UV-Vis spectral analysis of plant extract at 70°C and 90°C in figure (4D), where the absorption peaks of plant extract decreased gradually with time at 70°C due to catalytic degradation of bio-organics of this extract. The intensity decrease was strong and drastic when temperature was elevated to 90°C, as the degradation was accelerated by heating and hence these experiments are recommended at low temperatures.

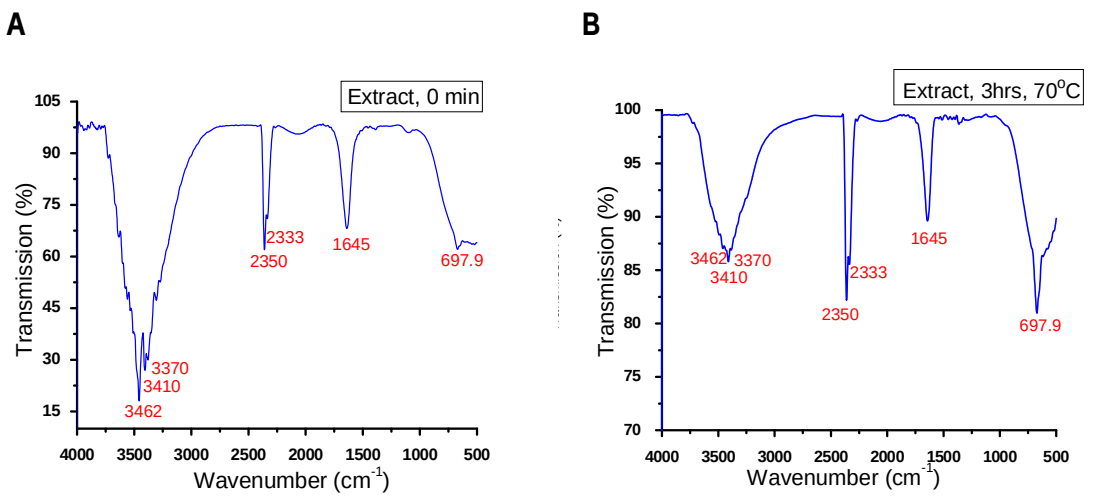

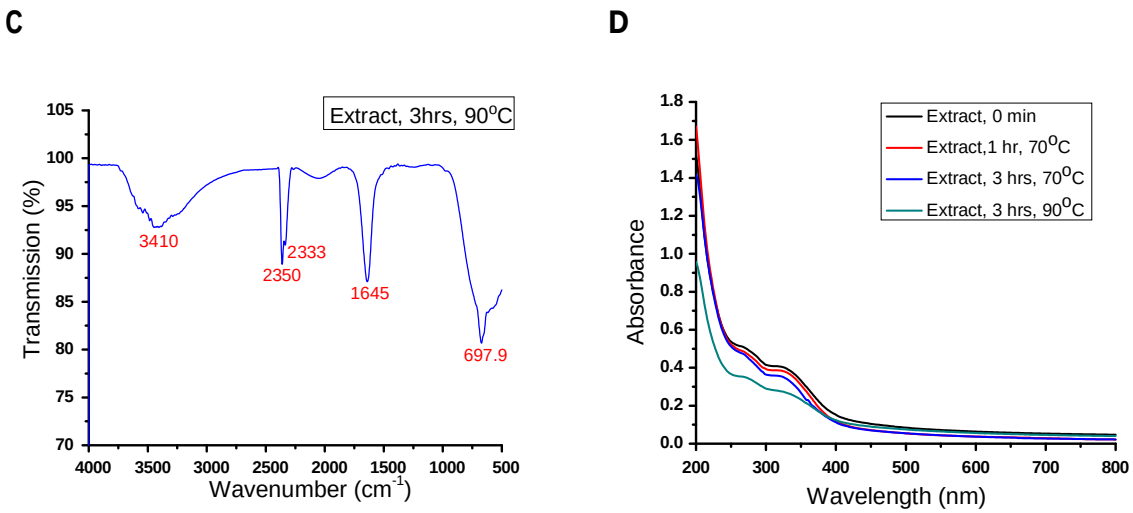

Figure 4. FTIR analysis of *Po* plant extract indicating presence of amino and hydroxyl groups (A), FTIR analysis of Po plant extract after 3 hours at 70°C which indicates the slight degradation of the extract (B), FTIR analysis of Po plant extract after 3 hours at 90°C where the degradation became more obvious (C), UV-Vis spectra of extract at different reaction parameters indicating decomposition of plant extract especially at 90°C (D).

Antibacterial activities of Ag-RGO nanocompsite. The time-dependent antibacterial effects of GO and Ag-RGO nanosheets were studied on E. coli 107 bacteria by using the colony counting method. A fixed amount of GO or Ag-RGO nanosheets were incubated with E. coli suspension for four hours, figure (5). Both GO and Ag-RGO demonstrated the same trend; the loss of cell viability increased gradually with increase in incubation time. The loss of cell viability of E. coli when incubated with GO nanosheets was 54±4.2% at the first hour. It increased gradually in the second and third hours to 68±3.9% and 79±4.5%, respectively. It reached its maximum as 87±5.1% at the fourth hour. On the other hand, Ag-RGO nanosheets exhibited a stronger antibacterial effect; the loss in cell viability at the first hour of incubation was 48±3.5%, the second and third hours were 73±5.2% and 85±4.7%, respectively. The fourth hour indicated a stronger effect as 92±4.1%.

The antibacterial effect of GO nanosheets was proved to be a combination of two main mechanisms; the first is the physical stress of sharp edges of GO nanosheets on cell wall and the second one was the oxidative stress (oxidation of some vital component in bacterial cells)[48, 49]. In addition, the antibacterial effect of AgNPs has many theories but the general understanding is morphological changes of bacterial cell wall (physical damage of membrane)[42,43] and the structural effects by reactive oxygen species (ROS), free radicals, interaction with sulfur-containing' membrane proteins with disturbing membrane permeability and interaction with phosphorous moieties of DNA, resulting in inhibition of DNA replication and prohibition of cell division.[44, 45]

The bio-organic reduction of GO-Ag suspension resulted in formation of Ag-RGO nanocomposite. Although RGO nanosheets have lower antibacterial effect than GO nanosheets, it was proven that the phytosynthesized Ag-RGO nanocomposite has a stronger antibacterial effect than GO nanosheets due to the synergetic harmony of action between AgNPs and RGO nanosheets.[61,62, 64]

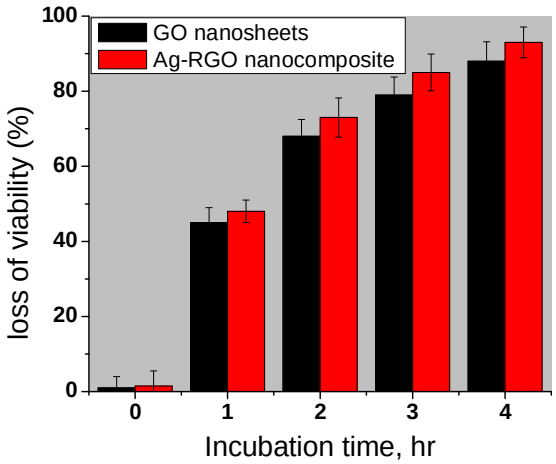

Figure 5. Loss of cell viability of E. coli when incubated with GO and Ag-RGO nanosheets. The loss increases with increase in incubation time

Conclusions:

In conclusion, a green and facile synthesis method was introduced for fabrication of Ag-RGO nanocomposite using the aqueous extract of *Potamogeton Pectinitus* (*Po*) plant. This is the first work to introduce *Po* as a reducing and capping agent in synthesis of Ag-RGO nanosheets. TEM analysis proved formation of the aforementioned nanocomposite and the homogenized distribution of AgNPs on surface of RGO nanosheets. The XRD analysis indicated partial reduction of GO nanosheets in GO-Ag suspension into Ag-RGO. FTIR analysis of *Po* plant extract demonstrated role of amine and hydroxyl groups of proteins, carbohydrates and other long chain compounds in reduction process. In the same context, a strong effect of reaction temperature on synthesis procedure due to its acceleration for catalytic degradation effect of GO or Ag-RGO on plant extract was demonstrated. On the other hand, the green synthesized Ag-RGO nanocomposite demonstrated a stronger antibacterial effect, against E. coli bacteria, than GO nanosheets. This was attributed to the synergetic effect of both AgNPs and RGO nanosheets.This antibacterial measurement is just a preliminary test to prove the enhanced antibacterial effect and a more detailed study is recommended.

Acknowledgments:

We would like to acknowledge Nile University for funding. We acknowledge also Department of Environmental science, Faculty of science, Alexandria university and Nanotech Egypt for photoelctronics where the experiments were done. Finally we thank Dr. Nahla Elkadi, Dr. Omer Elsheikh, Ali Abdo, Mahmoud Gamal and Ayman Amin for their help in experiments and allowance of bench space.

Notes and references

† Nanotechnology Centre, Nile University, Smart Village, B2-Km 28, Cairo-Alex Desert Road, Giza 12677, Egypt

‡ Faculty of Science, Botany Department, Sohag University, Sohag, Egypt

§ Faculty of Science, Environmental Sciences Department, Alexandria University, 21511 Moharram Bek, Alexandria, Egypt

‖ The National Institute of Laser Enhanced Sciences, Cairo University, Cairo, Egypt

Corresponding Author

* E-mail: mabdel-mottaleb@nileuniversity.edu.eg.

Notes

The authors declare no competing financial interest.

References:

(1) M. Mazur, Electrochemistry Communications, 2004, 6, 400.
(2) C. Baker, A. Pradhan, L. Pakstis, D. Pochan, and S. Shah, J. Nanosci. Nanotechnol., 2005, 5, 224.
(3) Y. W. Cao, R. Jin and, C. A. Mirkin, J. Am. Chem. Soc, 2001, 123, 7961.
(4) L. T. Chang and C. C. Yen, J. Appl. Polym. Sci., 1995, 55, 371.
(5) A. R. Shahverdi, S. Mianaeian, H. R. Shahverdi, H. Jamalifar and A. A. Nohi, Process Biochem., 2007, 42, 919.
(6) P. Matejka, B. Vlckova, J. Vohildal, P. Pancoska and V. Baumuruk, J. Phys. Chem., 1992, 96, 1361.
(7) M. P. Pileni, Pure Appl. Chem., 2000, 72, 53.
(8) K. Esumi, T. Tano, K. Torigoe and K. Meguro, J. Chem. Mater., 1990, 2, 564.
(9) A. Henglein, J. Phys. Chem. B, 1993, 97, 5457.
(10) A. Henglein, J. Chem. Mater., 1998, 10, 444.
(11) A. Henglein, Langmuir, 2001, 17, 2329.
(12) L. M. Liz-Marzan and I. Lado-Torino, Langmuir, 1996, 12, 3585.
(13) Y. S. Jae and S. K Beom, Bioprocess Biosyst. Eng., 2009, 32, 79.
(14) H. A. Kantrud, A Literature Review, Version 16JUL97; U.S. Fish and Wildlife Service, Fish and Wildlife Resource Publication 176; Northern Prairie Wildlife Research Center: Jamestown, ND, 1990. http://www.npwrc.usgs.gov/ resource/plants/pondweed/index.htm.
(15) L. Boulos, Al-Hadara Publishing: Egypt, 2005, 4, 330.
(16) D. Mhamane, Green Chem., 2011,13, 1990.
(17) A. AbdelHamid, M. Al-Ghobashy, M. Fawzy, M. Mohamed, M. Abdel-Mottaleb, *ACS Sustainable Chem. Eng*., 2013, 1, 1520.
(18)https://www.google.com.eg/search?q=potamogeton+pectinatus+plant&noj=1&tbm=isch&tb&source=univ&sa=X&ei=4HMhU2BI4H8ygPV9YKYBA&ved=0CC0QsAQ&biw=1366&bih=664. Retrieved: 12/03/2014.
(19) A. Kumar, V. Meena, S. Chattobadhyay, and K. Panigrahi, International Journal of Life Science & Pharma Reserch, 2012, 2, 2250.
(20) A. I. Lukman, B. Gong, C. E. Marjo, U. Roessner and A. T. Harris, J. Colloid Interface Sci., 2011, 353, 433.
(21) V. Kumar, S. C. Yaday and S. K. Yadav, J. Chem. Technol. Biotechnol., 2010, 85, 1301.
(22) Ahmad et al, Colloids Surface, 2010, 19, 81.
(23) K. K. Panda et al, Toxicol. In Vitro, 2011, 25, 1097.
(24) R. K. Das, B. B. Borthakur, U. Bora, Mater. Lett., 2010, 64, 1445.
(25) A. D. Dwivedi and K. Gopal, Colloids Surf., A, 2010 , 369, 27 .
(26) H. Bar, D. K. Bhui, G. P. Sahoo, P. Sarkar, S. Pyne, A. Misra, Colloids Surf., A, 2009, 348, 212.
(27) D. S. Sheny, J. Mathew and D. Philip, Spectrochim. Acta, Part A, 2011, 79, 254.
(28) D. Philip, Spectrochim. Acta, Part A, 2009, 73, 374.
(29) S. L. Smitha, D. Philip and K. G. Gopchandran, Spectrochim. Acta, Part A, 2009, 74,735.
(30) V. T. P. Vinod, P. Saravanan, B. Sreedhar, D. K. Devi and R. B. Sashidhar, Colloids Surf., B, 2011, 83, 291.
(31) G. Singhal, R. Bhavesh, K. Kasariya, A. Sharma and R. Singh, J. Nanopart. Res., 2011, 13, 2981.
(32) Centers for Disease Control and Prevention (CDC), Morb Mortal Wkly Rep (MMWR), 2013, 62, 165.
(33) R. Laxminarayan, D. L. Heymann, BMJ, 2012, 344, 1567.
(34) E. P.Abraham, E. Chain, Rev. Infect. Dis.,1988, 10, 677.
(35) J. Davies, and D. Davies, Microbiol Mol Biol Rev. 2003, 74, 417.
(36) K. K. Holmes, D. W. Johnson, T. M. Floyd, JAMA. 1967, 204, 61.
(37) G. Zhao, J. R. Stevens, Biometals, 1998, 11, 27.
(38) Aymonier et al, Chem Commun (Camb), 2002, 24, 3018.
(39) Lok et al, J. Proteome Res., 2006, 5, 916.
(40) M. Catauro, M. G. Raucci, F. D. Gaetano, A. Marotta, J. Mater Sci. Mater Med., 2004, 15, 831.
(41) J. H. Crabtree, R. J. Burchette, R. A. Siddiqi, I. T. Huen, L. L. Handott and A. Fishman, Perit Dial Int., 2003, 23, 368.
(42) J. R. Morones, J. L. Elechiguerra, A. Camacho, K. Holt, J. B. Kouri, and M. J. Yacaman, Nanotechnology, 2005, 16, 2346.
(43) I. Sondi and B. Salopek-Sondi, J. Colloid. Interface Sci., 2004, 275, 177.
(44) A. Gupta, Nat. Biotechnol., 1998, 16, 888.
(45) Y. Matsumura, K. Yoshikata, S. Kunisaki, T. Tsuchido, Appl. Environ. Microbiol., 2003, 69, 4278.

(46) Kim et al, Nanomed-Nanotechnol., 2007, 3, 95.
(47) L. Yu, Y. Zhang, B. Zhang, J. Liu, H. Zhang, C. Song, Journal of Membrane Science 447, 452-462
(48) Hu et al, ACS Nano, 2010, 4, 4317.
(49) Shaobin et al, ACS Nano, 2011, 9, 6971.
(50) A. Gupta, Nat. Biotechnol, 1998, 16, 888.
(51) Y. Matsumura, K. Yoshikata, S. Kunisaki, T. Tsuchido, Appl. Environ. Microbiol., 2003, 69, 4278.
(52) MARCANO et al, ACS NANO, 2010, 4, 4806.
(53) C. Hontoria-Lucas, A. J. Lo´pez-Peinando, J. Lo´pez-Gonza´lez, M. L. Rojas-Cervantes and R. M. Martı´n-Aranda,. Carbon, 1995, 320, 1585.
(54) C. Fu, G. Zhao, H. Zhang, S. Li, Int. J. Electrochem. Sci., 2013, 353, 6269.
(55) Lucchese et al, Carbon, 2010, 48, 1592.
(56) Y. N. Xia, J. A. Rogers, K. E. Paul and G. M. Whitesides, Chem. Rev., 1999, 99, 1823.
(57) B. Wiley, Y. Sun, B. Mayers and Y. Xia, European Journal, 2005, 11, 454.
(58) C. L. Haynes and R. P. Van-Duyne, J. Phys. Chem. B , 2001, 105, 5599.
(59) Treossi et al, J. Am. Chem. Soc., 2009, 131, 15576.
(60) J. Kim, L. J. Cote, F. Kim, J. Huang, J. Am. Chem. Soc., 2010, 132, 260.
(61) Xu et al, J Mater Chem, 2011, 21, 4593.
(62) J. Ma, J. Zhang, Z. Xiong, Y. Yong, X. S. Zhao, J. Mater. Chem., 2011, 21, 3350.
(63) M. R. Das, R. K. Sarma, R. Saikia, V. S. Kale, M. V. Shelke, P. Sengupta, J. Colloids Surfs B 2011, 83, 16–22.
(64) L. Yu, Y. Zhang, B. Zhang, J. Liu, J. Scientific Rep. 2014, 4, 4551.